BUBBLE FORMATION AT A SINGLE ORIFICE IN HIGHLY VISCOUS LIQUIDS

KOICHI TERASAKA AND HIDEKI TSUGE
Department of Applied Chemistry, Keio University, Yokohama 223

Key Words: Bubble, Bubble Formation, Bubble Formation Model, Highly Viscous Liquid

Bubble formation at an orifice submerged in highly viscous liquid was studied. The volume and shape of the bubble formed at an orifice and the pressure fluctuation in the gas chamber were measured experimentally. A revised nonspherical bubble formation model is proposed to describe the bubble formation mechanism and to estimate the bubble volume and shape and the pressure change in the gas chamber. The bubble volume, bubble shape and gas chamber pressure calculated by the present model agreed relatively well with the values obtained experimentally in a wide range of viscosity: $\mu=0.001$ to 1.1 Pas.

Introduction

It is essential in the design of gas-liquid contacting equipment such as fermentors or gas-phase polymerization reactors to clarify the formation of bubbles at an orifice submerged in highly viscous liquids. Many works of gas blowing operations from a submerged single orifice have been reported. To estimate the volume of the bubble formed at an orifice, some dimensionless correlation equations have been obtained.[7] While these equations give only the final bubble volume under various operating conditions, they do not describe the bubble volume and shape during bubble growth. Therefore, a number of bubble formation models have been proposed.[7]

Kupferberg and Jameson,[1] McCann and Prince,[3] and Tsuge and Hibino[6] have presented spherical bubble formation models to estimate the bubble volume formed in low-viscosity liquids. All these models require the final length of bubble neck obtained experimentally as the detachment condition. In the case of bubble formation in highly viscous liquids, however, it is difficult to determine the bubble neck length clearly owing to the deviation of bubbles from spherical shape.

On the other hand, a nonspherical bubble formation model does not require the detachment condition. Marmur and Rubin[2] and Pinczewski[5] have reported nonspherical models. Marmur *et al.*[2] did not consider the effect of liquid viscosity on bubble formation. Pinczewski[5] estimated well the volumes and shapes of bubbles formed in low-viscosity liquids by using a modified Rayleigh equation, but the volumes of the bubbles formed in highly viscous liquid as calculated by his model were much smaller than the experimental values because of the neglect of the viscous resistance of the rising bubble.

The objective of the present work is to propose a revised nonspherical model that describes the experimental results better than does the previous model[5] for a wide range of liquid viscosity. The main revised points are the inclusion of a viscosity term in the motion equation for the rising bubble and a modification in the definition of equivalent radii.

1. Bubble Formation Model

A bubble begins to grow at an orifice when the pressure in the gas chamber is larger than the sum of hydrostatic pressure and surface tension. The bubble surface moves by the pressure difference between the inside and the outside of the bubble. The bubble rises during bubble growth, and the bubble neck is formed in the final period of bubble growth. The bubble detaches itself when the bubble neck is closed.

1) Equivalent radii The bubble surface is divided into a number of two-dimensional axisymmetric elements which are characterized by two principal radii of curvature R and R' as shown in **Fig. 1**. R' is the radius of the circle which has the center O and passes through the elements $j-1$, j, and $j+1$, and the other radius R is the distance from the bubble's symmetrical axis to the element j through the point O.

In the present model, the pressure balance on each element is calculated by the same modified Rayleigh equation as is used in Pinczewski's model. Pinczewski[5] used the equivalent radius $\bar{R}$ defined by Eq. (1) as the characteristic radius.

$$1/\bar{R}=(1/R+1/R')/2 \tag{1}$$

However, the forces other than surface tension depend on the volume or mass of the bubble rather than the curvature of the bubble surface, so that $\bar{R}$ is used for

* Received June 8, 1989. Correspondence concerning this article should be addressed to H. Tsuge.

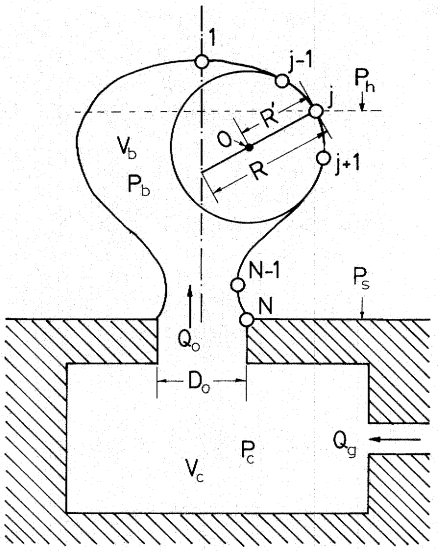

Fig. 1. Schematic diagram of nonspherical bubble formation model

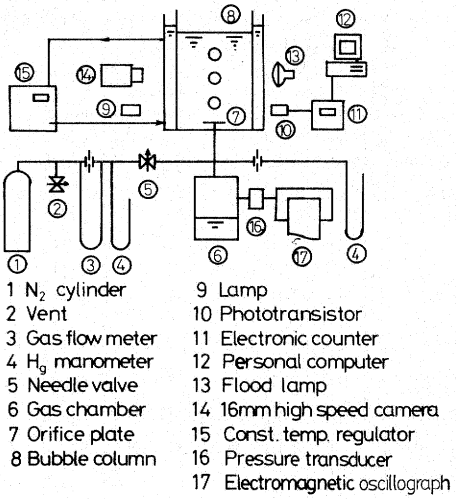

Fig. 2. Schematic diagram of experimental apparatus

surface tension and R is used for inertial and viscous forces as the characteristic radius in the present model.

2) Pressure change in the gas chamber When the behavior of gas in the gas chamber is assumed to be polytropic, the pressure change in the gas chamber during the bubble formation is expressed as

$$dP_c/dt=\kappa P_c(Q_g-Q_o)/V_c=\kappa P_c(Q_g-dV_b/dt)/V_c \quad (2)$$

where Q_g, Q_o, P_c, V_b, V_c and κ are gas flow rate into gas chamber, gas flow rate through an orifice, pressure in gas chamber, bubble volume, gas chamber volume and polytropic coefficient respectively. A polytropic coefficient κ is defined between 1 for isothermal change and 1.4 for adiabatic change of diatomic gases.

Kupferberg *et al.*[1] and McCann *et al.*[3] assumed that the gas behavior in the gas chamber changes adiabatically, whereas Park *et al.*[4] showed experimentally that polytropic coefficient κ is nearly 1.1.

3) Orifice Equation The pressure in the bubble P_b is related to P_c by the orifice equation as follows:

$$|P_c-P_b|=(Q_o/k_o)^2=(dV_b/dt)^2/k_o^2 \quad (3)$$

The orifice constant k_o is decided experimentally.

4) Pressure balance on gas-liquid interface The present model includes the following assumptions.

(a) The bubble is symmetrical about the vertical axis of the orifice.

(b) The bubble motion is not affected by the presence of the other bubbles.

On the element j, it is supposed that the bubble shape is a sphere with radius R. The expansion of the gas-liquid interface is written by the following modified Rayleigh equation:

$$P_b-P_h=\rho_l\left[R\frac{d^2R}{dt^2}+\frac{3}{2}\left(\frac{dR}{dt}\right)^2\right]+\frac{2\sigma}{\bar{R}}+\frac{4\mu dR}{Rdt} \quad (4)$$

where P_h is the hydrostatic pressure at the element j and the three terms on the right-hand side of Eq. (4) represent inertial, surface tension and viscous force respectively.

5) Motion equation of rising bubble The present model, obtained by revising Pinczewski's model,[5] includes the liquid viscous resistance of the rising bubble. The motion equation of a rising bubble is described by inertial, buoyancy, and viscous drag forces and gas momentum rate through an orifice as follows:

$$\frac{d}{dt}\left(M'\frac{dz}{dt}\right)=(\rho_l-\rho_g)V_bg-\frac{1}{8}C_D\rho_l\left(\frac{dz}{dt}\right)^2\pi D_m^2+\frac{4\rho_gQ_o^2}{\pi D_o^2} \quad (5)$$

where M' is virtual mass ($=(\rho_g+11\rho_l/16)V_b$) and C_D is the drag coefficient, which is a function of the Reynolds number. D_m is the maximum horizontal diameter of the bubble and is used as the charactristic diameter of a rising bubble.

The bubble surface expands and the bubble rises according to Eq. (4) and Eq. (5) respectively. When any element other than the apex of the bubble touches the vertical axis, the bubble detaches from the orifice. To solve the present model numerically, the finite-difference procedure is used as shown in Appendix.

2. Experimental Procedure and Conditions

Figure 2 shows the experimental apparatus. The bubble column has a 0.15 m square cross section and is 0.4 m in height. Assuming that the size of the bubble is uniform, a single bubble volume was calculated by dividing gas flow rate by the frequency of bubble formation measured by a phototransistor. The bubble shapes during bubble formation were photographed by a 16 mm high-speed camera (Locam Model 51: Red

Table 1. Physical properties of liquids

Liquid	$\rho_l \times 10^{-3}$ [kg/m^3]	μ [mPas]	σ [mN/m]	Mo [—]	T_l [K]
Distilled water	0.997	0.874	71.8	1.55×10^{-11}	299.0
90 wt% glycerol	1.235	118	59.4	7.34×10^{-3}	303.0
92 wt% glycerol	1.238	154	61.1	1.95×10^{-2}	296.3
Glycerol	1.257	812	61.3	1.51×10^{1}	298.0
Glycerol	1.260	1110	62.2	5.15×10^{1}	293.5

Lake Co.), and the bubble volumes were analyzed as a function of time with a film analyzer (Filmotion: Bell & Howell Co.). The pressure in the gas chamber was measured with a pressure transducer (Model 239: Setra Systems Inc.) and was recorded with a electromagnetic oscillograph (Model 2931 Photocorder: Yokogawa Electric Works).

The operating conditions were as follows: gas flow rate $Q_g = 0.1\text{–}10 \times 10^{-6}$ m^3/s, orifice diameter $D_o =$ 0.8–2.0 mm, gas chamber volume $V_c = 34\text{–}300 \times 10^{-6}$ m^3 and liquid height $H_l = 0.20$ m.

The orifice coefficient k_o was obtained experimentally as

$$k_o = 0.813 D_o^2 \tag{6}$$

where the units of k_o and D_o are m$^{7/2}$/kg$^{1/2}$ and m, respectively.

The polytropic coefficient κ obtained experimentally in this study was 1.1, which agrees with the experimental result by Park *et al.*[4]

Liquids used were distilled water, glycerol aqueous solutions and glycerol. Their physical properties are shown in **Table 1**.

3. Results and Discussion

3.1. Bubble growth curve and bubble shape change

Figures 3(a) and **(b)** show photographs of bubble formation in 92 wt% glycerol aqueous solution in the case of $V_c = 43 \times 10^{-6}$ and 301×10^{-6} m^3, respectively. It was observed that the bubble shape deviates from spherical with bubble growth. **Figure 4** shows a comparison of the bubble shape traced from photographs with that calculated by the present model during bubble formation in glycerol. The present model estimates well the experimental bubble shapes.

Figure 5 shows bubble growth and gas chamber pressure change curves in distilled water as a parameter of gas chamber volume for the conditions of $D_o = 1.47$ mm and $Q_g = 0.21 \times 10^{-6}$ m^3/s. In the case of small V_c, bubble volume decreases after it reaches maximum value. **Figures 6** and **7** shows bubble growth and gas chamber pressure change curves in 92 wt% glycerol aqueous solution and glycerol, respectively, as a parameter of gas chamber volume V_c for the conditions of $D_o = 1.47$ mm and $Q_g = 1.1 \times 10^{-6}$ m^3/s.

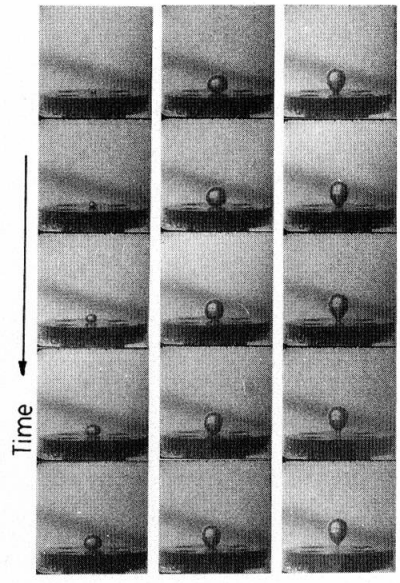

Fig. 3(a). Bubble formation photographed at 200 frames/s by high-speed camera ($V_c = 42.5 \times 10^{-6}$ m^3, $D_o = 1.47$ mm, N_2-92 wt% glycerol aqueous solution system)

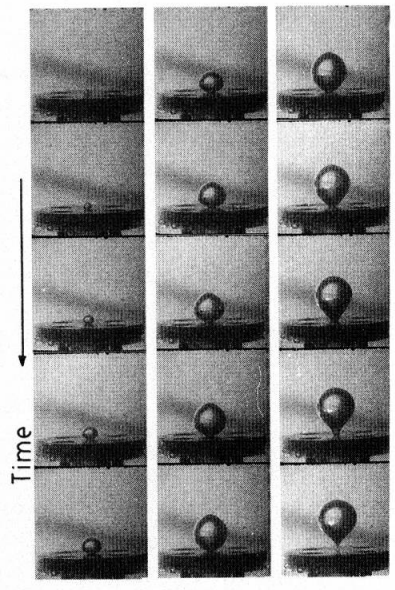

Fig. 3(b). Bubble formation photographed at 200 frames/s by high-speed camera ($V_c = 300.5 \times 10^{-6}$ m^3, $D_o = 1.47$ mm, N_2-92 wt% glycerol aqueous solution system)

As shown in Figs. 5–7, bubbles expand rapidly with rapid decrease of gas chamber pressure at first. In the case of the relatively low-viscosity liquids shown in Figs. 5–6, bubbles detach after sudden decrease in pressure. On the other hand, in the case of the highly viscous liquid shown in Fig. 7, bubbles grow continuously with sudden and then gradual decreases of gas chamber pressure, and at last detach. Therefore, with the same operating condition and equipment, the bubble formation time in highly viscous liquids is much longer than that in low-viscosity liquids. The computed results shown by the lines in Figs. 5–7 are

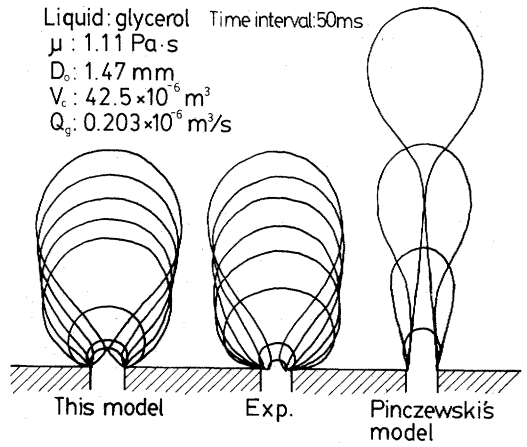

Fig. 4. Comparison of bubble shapes given by experiment, the present model and Pinczewski's model

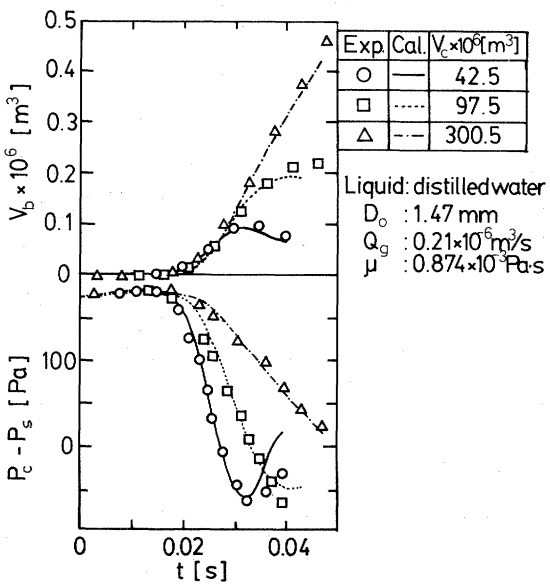

Fig. 5. Bubble volume and pressure change in gas chamber against bubble formation time

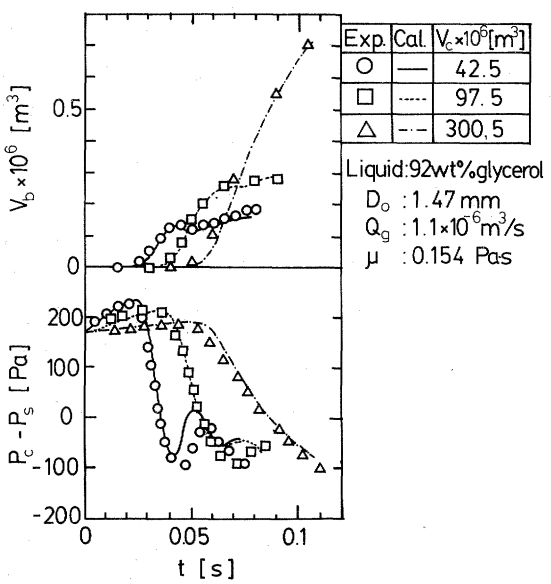

Fig. 6. Bubble volume and pressure change in gas chamber against bubble formation time

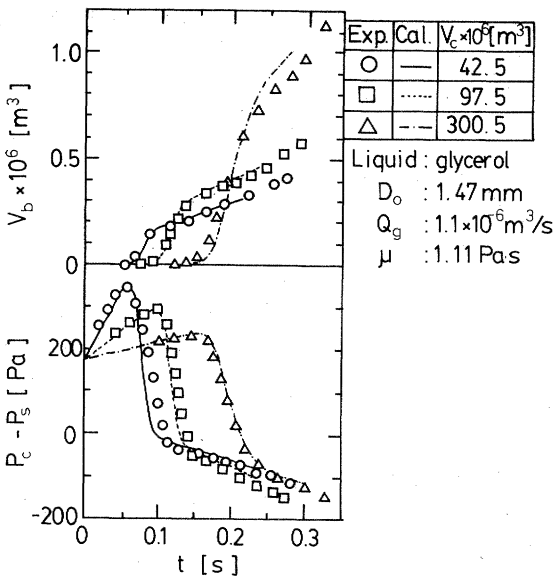

Fig. 7. Bubble volume and pressure change in gas chamber against bubble formation time

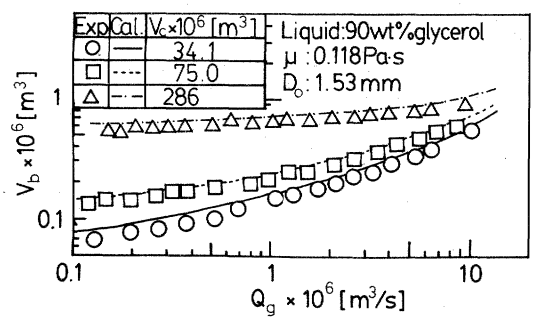

Fig. 8. Effect of gas chamber volume on relation between V_b and Q_g

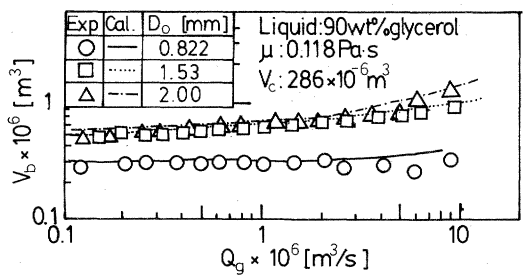

Fig. 9. Effect of orifice diameter on relation between V_b and Q_g

in good agreement with the experimental results. The computed gas chamber pressures are also in good agreement with the measured values.

3.2 Effect of various factors on bubble volume

Figure 8 shows the relation between V_b and Q_g with gas chamber volume V_c as a parameter. V_b increases with increase of V_c, but the effect becomes small.

Figure 9 shows the effect of orifice diameter D_o on V_b. Although V_b increases with increase of D_o, the difference of V_b between $D_o = 1.53$ and 2.00 mm is little.

Figure 10 shows the relation between V_b and Q_g with liquid viscosity μ as a parameter. V_b increases with increase of μ.

The computed results shown by the lines in Figs. 8–10 agree well with the experimental results for each parameter in Figs. 8–10.

3.3 Comparison with other researchers' results

To compare the present model with Pinczewski's model, the bubble shape by Pinczewski's model was calculated and is very different from the experimental one, as shown in Fig. 4. This is because the motion equation of the rising bubble in his model does not contain the viscous drag force term, so that the estimated rising velocity is much larger than the experimental one. As shown in **Fig. 11**, the bubble estimated by his model detaches from the orifice earlier than in the experimental results, so that the bubble volume is smaller than the experimental value and that calculated by the present model.

Figure 12 shows a comparison between the experimental results of bubble growth curve and pressure change in the gas chamber by Kupferberg *et al.*,[1] and the computed results by the present model. It shows good agreement even though the experimental conditions of Kupferberg *et al.* are considerably different from those of the present work, especially V_c and D_o.

Conclusions

The effects of gas flow rate, gas chamber volume, orifice diameter and liquid viscosity on the volumes of bubbles at an orifice submerged in highly viscous liquids were investigated experimentally. The bubble volumes increase with increase of V_c, D_o and μ.

By measuring simultaneously the changes in the bubble volume, the bubble shape and the pressure in the gas chamber during bubble growth, the bubble formation mechanism was investigated. It was found that the bubble formation time is much longer in highly viscous liquids than in low-viscosity liquids, so that the bubble volume is much larger.

To express physically the bubble formation at an orifice, a nonspherical bubble formation model obtained by revising Pinczewski's model was presented. The model estimated well the volume and shape of the bubble and the gas chamber pressure change during bubble growth in a wide range of liquid viscosity, from 0.001 to 1.1 Pas.

Appendix

To solve the nonspherical bubble formation model numerically, the following finite-difference procedure is used.

1) Initial conditions The initial bubble shape observed in this work was hemispherical, so that the bubble is assumed to be initially a hemisphere with radius equal to the orifice radius R_o. The velocities and accelerations of all elements are set to zero. The initial pressure in the gas chamber is set equal to the sum of hydrostatic pressure

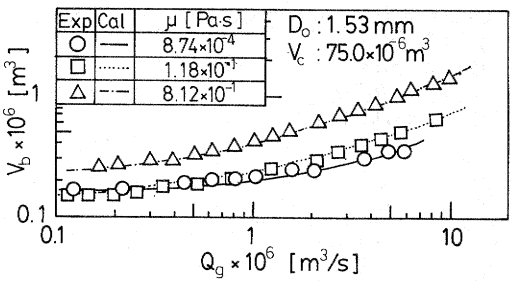

Fig. 10. Effect of liquid viscosity on relation between V_b and Q_g

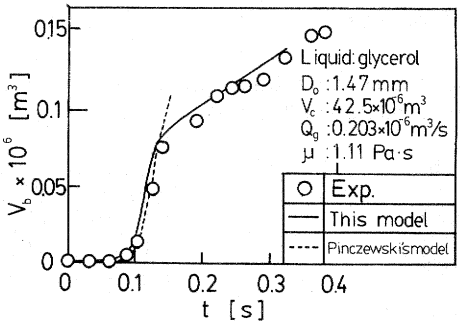

Fig. 11. Comparison between bubble growth curves by the present model and by Pinczewski's model

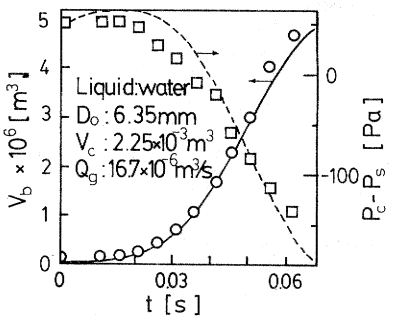

Fig. 12. Comparison of experimental data of Kupferberg *et al.* with results calculated by the present model

at the orifice and the surface tension as follows:

$$P_c|_0 = P_0 + \rho_l g H_l + 4\sigma/D_o \qquad \text{(A-1)}$$

where P_0 and H_l are atmospheric pressure and liquid height, respectively, and the symbol $|_t$ expresses the value at time t.

2) Boundary conditions

(a) The element of the bubble apex $j=1$ moves on the symmetrical axis of the bubble.

(b) The element contacting the orifice edge $j=N$ does not move, so that the velocity and acceleration of the element are usually zero.

(c) The bubble surface does not cross the orifice plate.

3) Finite-difference procedure

(a) The change in pressure in the gas chamber P_c in the time step Δt is described by

$$P_c|_{t+\Delta t} = P_c|_t - \kappa P_c|_t [V_b|_{t+\Delta t} - V_b|_t - Q_g \Delta t] V_c \qquad \text{(A-2)}$$

(b) The pressure in the bubble is obtained as

$$P_b|_{t+\Delta t} = P_c|_{t+\Delta t} - (dV_b/dt|_{t+\Delta t})^2/k_o^2 \qquad \text{(A-3)}$$

(c) The equivalent radii R and R' are calculated geometrically.

(d) The radial acceleration of each element in the time step Δt is described by

$$d^2R/dt^2|_{t+\Delta t}=[P_b|_{t+\Delta t}-P_h-3\rho_l(dR/dt|_t)^2/2 -2\sigma/\bar{R}|_t-4\mu dR/dt|_t/R|_t]/\rho_l R|_t \quad \text{(A-4)}$$

The radial velocity of each element is calculated from

$$dR/dt|_{t+\Delta t}=dR/dt|_t+d^2R/dt^2|_{t+\Delta t}\Delta t \quad \text{(A-5)}$$

The radial displacement of each element in time step Δt is

$$\Delta R|_{t+\Delta t}=[dR/dt|_t+d^2R/dt^2|_{t+\Delta t}\Delta t/2]\Delta t \quad \text{(A-6)}$$

(e) The vertical acceleration of the rising bubble is calculated as follows:

$$d^2z/dt^2|_{t+\Delta t}=[(\rho_l-\rho_g)V_bg-C_D\rho_l(dz/dt|_t)^2\pi D_m|_t^2/8 +4\rho_gQ_o^2/\pi D_o^2]/M'|_t-3dR/dt|_t dz/dt|_t/R|_t \quad \text{(A-7)}$$

The vertical velocity and displacement in Δt are described by

$$dz/dt|_{t+\Delta t}=dz/dt|_t+d^2z/dt^2|_{t+\Delta t}\Delta t \quad \text{(A-8)}$$

$$\Delta z|_{t+\Delta t}=[dz/dt|_t+d^2z/dt^2|_{t+\Delta t}\Delta t/2]\Delta t \quad \text{(A-9)}$$

(f) The bubble volume $V_b|_{t+\Delta t}$ is obtained by integrating the coordinates of all elements.

(g) The procedure is repeated for the next time step. Elements should be added with the increase of bubble surface area to express the bubble shape smoothly during bubble growth.

(h) The time step Δt should be chosen to minimize the calculating error. In the present computation, the time step used was between 1 and 50 μs.

Nomenclature

C_D	=	drag coefficient	[—]
D_m	=	maximum horizontal diameter of bubble	[m]
D_o	=	orifice diameter	[m]
g	=	gravitational acceleration	[m/s^2]
H_l	=	height of liquid	[m]
k_o	=	orifice constant	[m$^{7/2}$/kg$^{1/2}$]
M'	=	virtual mass ($=(11\rho_l/16+\rho_g)V_b$)	[kg]
Mo	=	Morton number ($=g\mu^4/\rho_l\sigma^3$)	[—]
P_b	=	pressure in bubble	[Pa]
P_h	=	hydrostatic pressure at element j	[Pa]
P_s	=	hydrostatic pressure at orifice plate	[Pa]
P_0	=	atmospheric pressure	[Pa]
Q_g	=	flow rate of gas into gas chamber	[m^3/s]
Q_o	=	flow rate of gas through an orifice	[m^3/s]
R and R'	=	principal radii of curvature	[m]
$\bar{R}$	=	mean bubble diameter defined by Eq. (1)	[m]
Re	=	Reynolds number ($=\rho_l D_m(dz/dt)/\mu$)	[—]
T_l	=	temperature of liquid	[K]
t	=	bubbling time	[s]
Δt	=	time step	[s]
V_b	=	bubble volume	[m^3]
V_c	=	gas chamber volume	[m^3]
z	=	vertical distance from orifice plate	[m]
κ	=	polytropic coefficient	[—]
μ	=	liquid viscosity	[Pas]
ρ_l	=	liquid density	[kg/m^3]
ρ_g	=	gas density	[kg/m^3]
σ	=	surface tension	[N/m]

Literature Cited

1) Kupferberg, A. and G. J. Jameson: *Trans. Instn. Chem. Engrs.*, **47**, T241 (1969).
2) Marmur, A. and E. Rubin: *Chem. Eng. Sci.*, **31**, 453 (1976).
3) McCann, D. J. and R. G. H. Prince: *Chem. Eng. Sci.*, **26**, 1505 (1971).
4) Park, Y., A. L. Tyler and N. de Nevers: *Chem. Eng. Sci.*, **32**, 907 (1977).
5) Pinczewski, W. V.: *Chem. Eng. Sci.*, **36**, 405 (1981).
6) Tsuge, H. and S. Hibino: *Chem. Eng. Commun.*, **22**, 63 (1983).
7) Tsuge, H.: Encyclopedia of Fluid Mechanics, **vol. 3**, p. 191, Gulf Publishing Co. (1986).